# Space Shuttle Redesigned Solid Rocket Motor Field Joint Verification

M. Perry,* N. Eddy,† L. Gruet,‡ and J. Maw§
*Thiokol Corporation, Brigham City, Utah 84302*

**The internal insulation in the Space Shuttle redesigned solid rocket motor field joint was designed to provide thermal protection to the steel case and O-ring seals. An unvented design concept was chosen to prevent hot chamber gases from reaching the inner joint. The joint design was verified through flow/thermal analyses and tests. Postulated flaws and subsequent leak paths through the joint bondline and O-ring seals were analyzed to verify that the joint would perform adequately under these undesired conditions. Tests of static motors with flawed joints paralleled the analysis effort, verifying design insensitivity to manufacturing flaws and subsequent leak paths. Results of tests and analyses showed that the design met all performance and safety requirements.**

## Nomenclature

$V_1$ = between CF O-ring and CF tip
$V_2$ = between CF and primary O-rings
$V_3$ = between the CF tip and the adhesive bond
$V_4$ = in the CF O-ring groove chamfer

## Introduction

THE Space Shuttle Discovery was successfully launched using two redesigned solid rocket motors (RSRMs) on September 29, 1988 (Fig. 1). A major modification to these RSRMs included the redesign of the field joints, where individual casting segments are joined to form the large 126-ft-long, 12-ft-diam motor. The steel case and the acrylonitrile butadiene rubber (NBR) insulation in the joint region were redesigned to increase the RSRM reliability. The thermal integrity of the redesigned field joint was verified through extensive testing and flow/thermal analyses.

Flaws were postulated which would breach the joint features designed to seal and thermally protect the joint as a part of the redesign process. These hypothetical flaws were analyzed extensively. Independent defects were compounded, resulting in flaws with increasing severity for purposes of analytic modeling and static testing. Analytical results were sought to verify that the joint would maintain a seal with acceptable levels of heat effect on the O-rings and the steel case. Static motors were tested in parallel with the analytical effort. Subscale motors were used first, starting with single flaws and evolving to compounded flaws. These tests provided the experience necessary to test flaws in full-scale short-burn duration motors, and eventually in full-scale RSRM static tests. These thermal analyses and flaw tests are discussed, following a description of the field joint design.

## Field Joint Design

The assembled RSRM is comprised of a steel case insulated with NBR rubber and filled with solid propellant an igniter, and a nozzle. The motor is manufactured as four casting segments for ease of handling and transportation (Fig. 2). The field joints are formed where the casting segments are joined at the launch site.

The key feature of the redesigned case was the addition of the capture feature (CF) to the tang (Fig. 3). It holds a third O-ring as a thermal barrier and provides an interference fit with the inner clevis leg. The interference fit minimizes movement of the steel case joint, enhancing the sealing capability of the primary and secondary O-rings. A fluorocarbon rubber insert, the $V_2$ volume fuller, was added to reduce the free volume between the CF O-ring and primary O-ring. The $V_2$ filler is inserted as eight pieces separated by 2-in. gaps. It occupies a minimum of 65% of the free volume and acts as a thermal barrier should leakage into the joint occur. Steel pins inserted into aligned holes in the clevis and tang hold the joint together.

Many design concepts for the field joint insulation were proposed and assessed.[1,2] Eventually the choice was narrowed to a bonded, unvented configuration where hot motor gases were not allowed to reach the O-ring seals (Fig. 3). Insulation

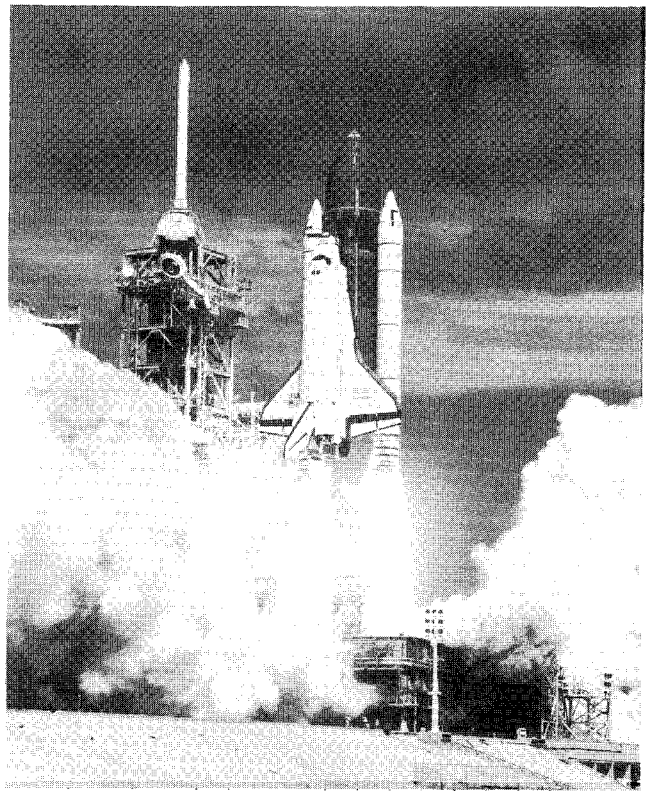

**Fig. 1 Space Shuttle Discovery lifts off, boosted by RSRMs.**

Presented as Paper 89-2775 at the AIAA/ASME/ASEE/SAE 25th Joint Propulsion Conference, Monterey, CA, July 10-12, 1989; received Sept. 22, 1989; revision received April 20, 1990; accepted for publication April 24, 1990. 

*Engineer, Insulation Design. Member AIAA.
†Associate Scientist, Insulation Design.
‡Engineer, Aero/Thermal.
§Scientist, Aero/Thermal.

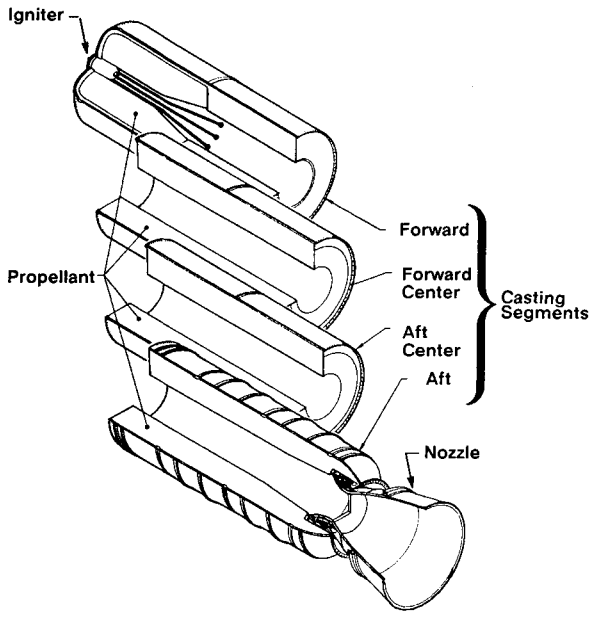


Fig. 2 RSRM casting segments.

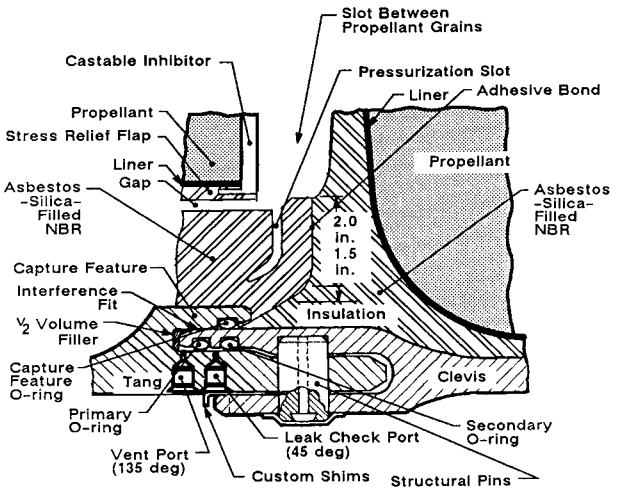


Fig. 3 RSRM field joint (J-joint).

on the tang side of the joint contains a pressurization slot forming an insulation flap (J-leg). The resiliency of this feature serves several important functions. It provides a means of accommodating insulation fabrication tolerances, thermal expansion or contraction, and propellant slump by maintaining insulation-to-insulation contact following joint assembly. The sealing capability of the joint is enhanced by motor pressure forcing the J-leg against the opposing clevis insulation. Adhesive was added to the mating surfaces of the J-joint to ensure that the J-leg remained in contact with the clevis insulation during prelaunch propellant grain temperature excursions and motor pressurization.

The J-joint design features multiple seals and thermal barriers. A defect in the J-joint bondline, the first barrier, can be supposed despite visual and dimensional inspections. This defect could result in a direct flow path to the CF O-ring. The CF O-ring acts as the next barrier to gas penetration if the bondline is breached. The third barrier is the steel case interference fit, and the fourth and fifth barriers are the primary and secondary O-ring seals. Defects in the CF O-ring, the metal-to-metal interference, and the primary and secondary O-rings are also possibilities, but simultaneous occurrences of these defects are statistically improbable.

Flow/thermal analyses and static motor tests were conducted to verify the thermal adequacy of joint.[3] Both the design case and the cases with postulated flaws were assessed.

## Design Verification

### Flow/Thermal Analyses

Flow/thermal analyses of the J-joint configuration investigated several scenarios, many of which were tested in subscale and fullscale motors. Three types of analyses were conducted: design case, single leak path, and double leak path.[4-7] The "leak paths" were assumed to evaluate the thermal integrity of the joint with unintended flaws.

The design case analysis assumed normal operation of the field joint insulation. Erosion and in-depth temperatures of the internal insulation were predicted in the vicinity of the joint. The thermal boundary conditions were based upon local flow conditions in the chamber.

The single leak path analyses dealt with heating and erosion caused by the entrance of chamber gases through a single leak path in the adhesive bondline. These analyses assumed flow past the CF O-ring, either from an assumed flaw or a predicted burnthrough.

The double leak path analyses studied circumferential flow adjacent to the CF O-ring. A pressure gradient may exist circumferentially at the field joint and induce gas flow between two bondline leak paths. Circumferential flow could be caused by a propellant slump due to horizontal storage and transportation prior to a vertical stacking at Kennedy Space Center.

The analyses did not consider more than two leak paths. Multiple leak paths resulted in reduced pressure gradients between the chamber and the free volumes, slower gas velocities through the leak paths, and shorter volume fill times. The resulting thermal effects would all be reduced under these conditions.

### Models

Three flow/thermal codes were used to conduct the analyses. The Charring Material and Ablation (CMA) program was used to predict the insulation erosion and in-depth temperature response in the design case. The in-house code ORING2[4] and the Systems Improved Numerical Differencing Analyzer (SINDA) were used to predict pressures, mass flow rates, O-ring erosion, and temperatures for the leak path analyses.

Definitions

$V_1$ —Between capture feature O-ring and capture feature tip

$V_2$ —Between capture feature and primary O-rings

$V_3$ —Between the capture feature tip and the adhesive bond

$V_{2A}$—In the capture feature O-ring groove chamfer

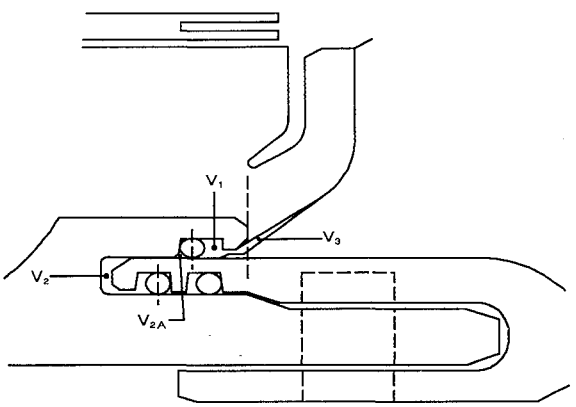


Fig. 4 RSRM field joint free-volume definitions.

The CMA program is a one-dimensional thermal code that assumes surface chemical equilibrium and decomposition properties to predict pyrolysis depth, char depth, decomposition rates, and temperature gradients throughout the model.

ORING2 predicts pressure rise rates in the free volumes, mass flow rates in the channel defects, gas temperatures, and jet impingement erosion of the O-rings. ORING2 accounts for jet spreading, flow path erosion, and geometric changes within the J-joint caused by motor pressurization. Erosion increases the cross section of the flow path and reduces the fill time. Motor pressurization compresses the J-leg reducing the $V_3$ free volume (Fig. 4).

The calculated mass flow rates from ORING2 were input into the three-dimensional thermal code SINDA to calculate the gas temperatures and the in-depth solid temperatures. Insulation erosion was indirectly accounted for by adjusting the gas temperature at the J-joint inlet until the resulting gas temperatures in front of the CF O-ring were similar to the gas temperatures predicted by ORING2. SINDA and ORING2 feature variable material properties and convective heat transfer coefficients.

### Design Case

All of the thermal effects occurred from local heating in the chamber. Thermal boundary conditions were applied at the base of the slot between propellant grains. This slot is located between the segments and is adjacent to the joint entrance (Fig. 3). The convective heating in the model was adjusted so that the resulting material-affected depth (MAD) agreed with the erosion measured in the static test of the fifth full-scale, full duration development motor (DM-5) of the old high-performance motor design. This correlation was used because of uncertainties in the flow field at the base of the slot. The convective heating environment was extended to the base of the pressurization slot, and the entrance radiation component was modified by an appropriate view factor.

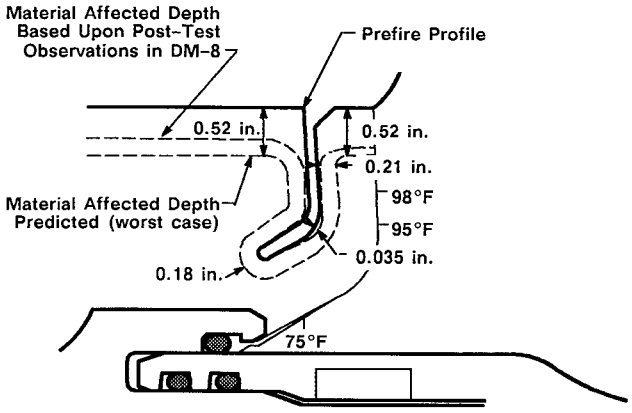


Fig. 5 Design case thermal results.

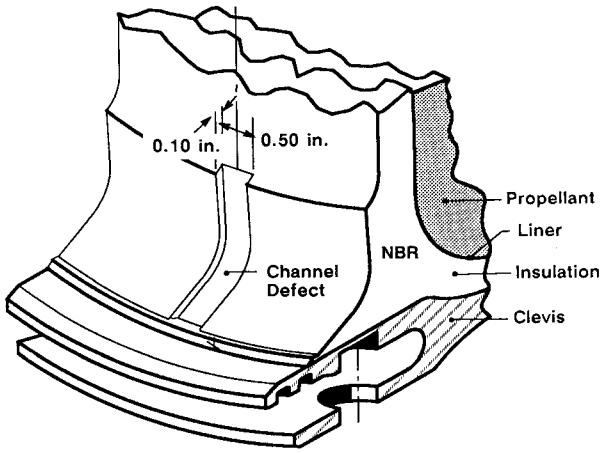


Fig. 6 J-joint channel defect.

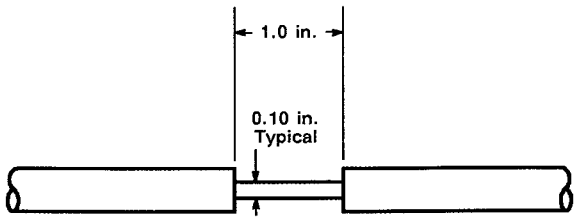


Fig. 7 O-ring cross-section reduction flaw.

The thermal results[4] for the design case are compared to the post-test observation of the DM-8 full-scale, full-duration static test in Fig. 5. All metal and O-ring temperature predictions remain at ambient during motor burn. At the elbow of the pressurization gap, where 0.21 in. of MAD was predicted, only 0.035 in. of MAD was measured in the DM-8 static test motor. This comparison indicated that the correct radiative heating environment was used in the analysis, but the convective heating environment was too severe. The DM-8 thermal results show that the gas flow at the base of the slot is predominantly in the axial direction and should not be extended to the base of the pressurization gap. The analysis served its purpose, however, it was conducted with a conservative convection assumption to ensure the O-rings and steel parts remained within design tolerances under severe conditions. Only soot and minimal amounts of char have been found in the pressurization slot from post-test inspections of other full-scale static test motors as in DM-8. The performance of the J-leg in full-scale, full-duration static tests has been satisfactory and the joint has functioned as designed.

### Single Leak Path

Three insulation bondline leak path dimensions were evaluated in the single leak path analyses: 0.016 × 0.250 in., 0.050 × 0.125 in., and 0.1 × 0.5 in. (Fig. 6).[4-7] NASA agreed that these leak path dimensions were both reasonable and conservative.

The RSRM J-joint was designed with an interference fit [63 $R_a$ (roughness average) finish] between the CF and the inner clevis leg (Fig. 3). The assembly tests of the joint indicated that the RSRM segments may be out-of-round and that gaps as large as 0.005 in. may exist between the CF and the inner clevis leg instead of the designed interference fit. Various "interference gaps" ranging from 0.000063 to 0.005 in. were analyzed to study the thermal effects of out-of-round segments.[5-7] These gaps were analyzed in conjunction with a breached capture feature O-ring (Fig. 7), situated in line with the insulation leak path.

Once hot gas was predicted to burn through the CF O-ring, the width and direction of the gas jet flowing through the interference gap depended on the height of the interference gap. A small interference gap has a large resistance to fluid flow, forcing the gas to flow circumferentially beside the CF O-ring and pressurize a small free volume called $V_2A$ in Fig. 4. $V_2A$ is located directly adjacent to the capture feature O-ring. Once this small free volume attains enough pressure to overcome the flow resistance in the interference fit, the $V_2$ volume is pressurized uniformly around the complete circumference of the field joint, rather than by a gas jet of a restricted width. The flow resistance is reduced and the $V_2$ volume is pressurized by a gas jet of a more restricted width for larger interference gaps.

Large interference gaps only occur if the joining segments are out-of-round for circumferential distances less than 2.5 in. Structural analyses show that if an interference gap occurs for a significant width, greater than 2.5 in., ignition pressure will close this gap to an interference fit during motor burn.

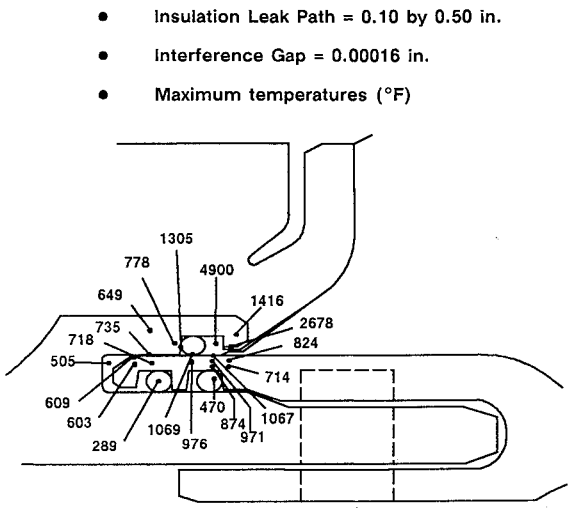


**Fig. 8 Single leak path thermal results.**

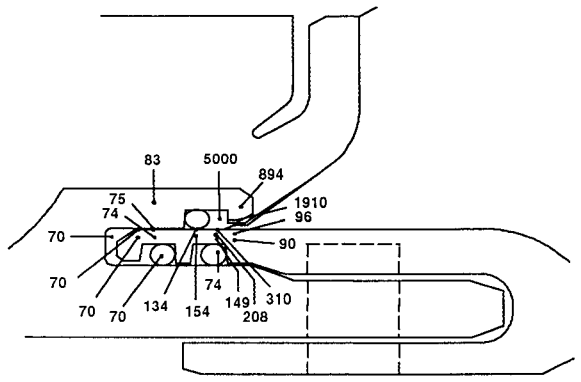


**Fig. 9 Double leak path thermal results.**

A full circumference jet width was used to fill the $V_2$ volume for interference gap heights of 0.00016 in. or less. The width of the gas jet filling $V_2$ was assumed equal to the flaw dimensions of the CF O-ring for the analyses with larger interference gaps.

The thermal results[6] of a typical analysis where the 0.1 × 0.5 in. insulation bondline leak path was used (Fig. 6) are shown in Fig. 8. The CF O-ring had a 1.0-in.-wide insulation flaw, similar to the one shown in Fig. 7. A 0.00016-in. interference gap was assumed. All of the temperatures are maximum values and are very localized, dropping significantly in the circumferential direction. The gas temperature is predicted to decrease from 4900°F in the $V_1$ cavity to 505°F at the entrance of the $V_2$ volume. Additional heat is lost as the gas must flow past the $V_2$ filler to reach the primary O-ring. The jet impingement and gas flow into the $V_2$ volume was great enough to predict the reduced CF O-ring to burn through. The steel temperatures were predicted to be well below the melting point of 2760°F, and the Viton primary and secondary O-rings were predicted to be below their ablation temperature of 805°F.

In summary, the results of flow/thermal analyses for a single leak path show the J-joint will perform satisfactorily even with in-line insulation bondline and CF O-ring flaws. However, a large interference gap with a narrow width (less than 2.5 in.) may pose a problem. A narrow gap will not close during motor pressurization; it could result in hot gases in the $V_2$ volume, melted steel, and primary O-ring erosion from jet impingement or conduction through the clevis steel. Primary O-ring damage from jet impingement will occur only if gas flow through a small single leak path is capable of burning through the CF O-ring, and is in direct alignment with such an interference gap and one of the seven $V_2$ filler gaps. The analyses indicate the hot gas may partially damage the clevis leg, but the joint will not fail during motor operation. Many preflight tests and inspections are conducted to prevent such an occurrence.

### Double Leak Path

The double leak path analyses dealt with the effects of gas flow along the CF O-ring resulting from two leak paths and a circumferential pressure gradient in the motor chamber. Both leak paths were assumed to have the same dimensions, 0.016 × 0.250 in., and to be spaced 160 deg apart.

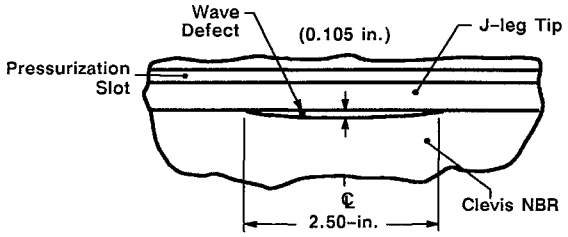


View A-A (rotated 90 deg)

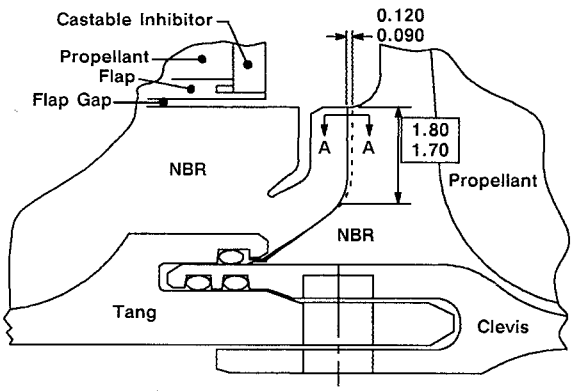


**Fig. 10 Field joint wave defect.**

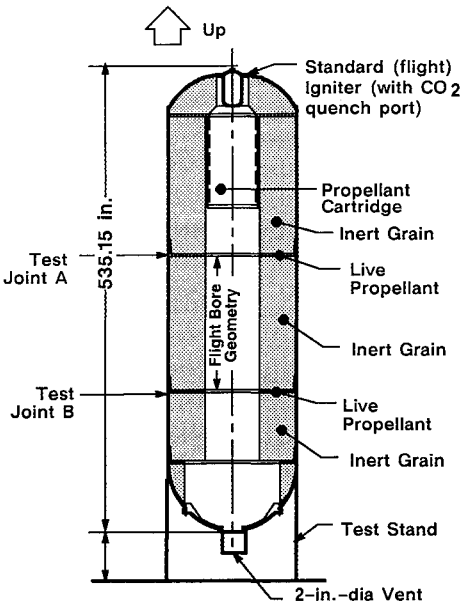


**Fig. 11 Joint environment simulator.**

**Table 1 Type 1 defects to the capture feature O-ring**

| | Defect configuration circumference × width, in. | Thermal results: Erosion of capture[b] feature O-ring, in. | | Thermal results: Metal damage[c] | |
|---|---|---|---|---|---|
| Test article | J-joint defect | Predicted | Measured | Predicted | Measured |
| JES-3A[a] (joint B) | Wave: 2.5 × 0.105 | None | None | None | None |
| JES-3B (joint A) | Channel: 0.125 × 0.05 | 0.150 | 0.138 | None | None |
| QM-6 (center joint) | Wave: 2.5 × 0.105 | None | None | None | None |
| PVM-1 (center joint) | Channel: 0.125 × 0.05 | 0.280 | 0.252 | None | None |

[a]The wave defect sealed during motor pressurization. [b]Diametrical erosion. [c]Steel temperature greater than 1000°F.

The thermal results[4] of the double leak path analysis are shown in Fig. 9. The maximum temperatures were lower than the values predicted for the single leak path due to the reduced $V_1$ and $V_3$ volume fill time. The greatest heating occurred during the volume filling. The convection heating from the circumferential gas flow was insignificant because of low gas velocity.

**Flaw Testing**

Flaws were implemented in the insulation bondline, the O-rings, and the interference fit hardware to support and verify flow/thermal analytical efforts.

Bondline flaws were configured as channels or waves to facilitate analytical modeling and testing. These channels were rectangular, had constant cross sections, and ran the length of the mating J-joint surface (Fig. 6). They were intended to guarantee leakage through the J-joint bondline. Wave defects had the cross section of a half sine wave (Fig. 10). These were configured to represent potential true manufacturing defects and tested to determine if they would close during ignition pressurization.

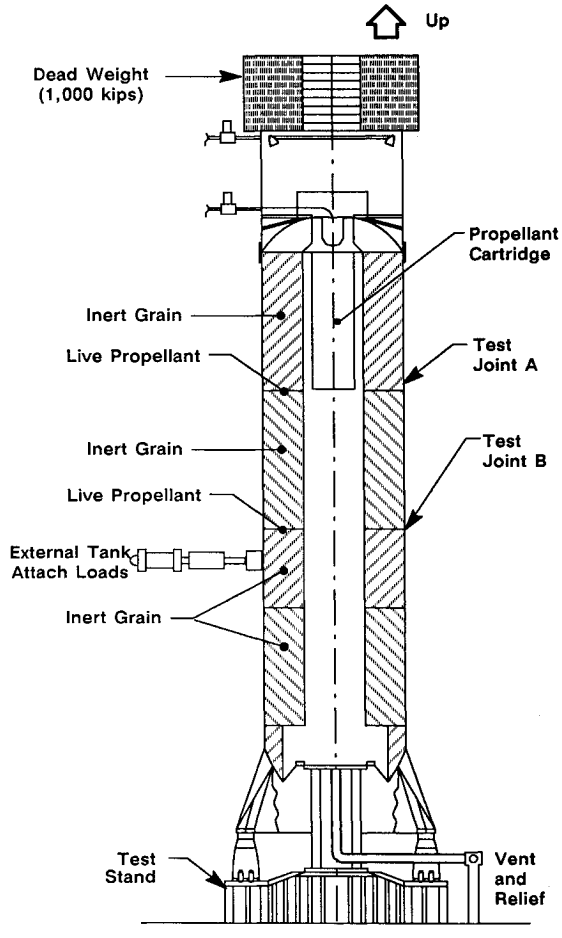


**Fig. 12 Transient pressure test article.**

O-ring defects were simulated by reduced cross sections (Fig. 7), seal surface contamination, and in one case by slicing the CF O-ring to a 0.09-in. depth over a 6-ft length. Reduction of the cross section was intended to guarantee leakage past the O-ring. These flaws were tested to demonstrate joint design tolerance to O-ring defects.

Both wide and narrow interference gaps were tested. The wide case had a 0.005–0.010-in. gap over the full circumference. The narrow case had a 0.005–0.010-in. gap over a 2-in. circumference.

*Test Motors*

These defects were investigated in a series of precedence-setting solid rocket motor (SRM) tests. Defects were initially tested in seventy-pound charge (SPC) subscale motors, then in full-diameter, short-burn duration test vehicles, the joint environment simulator (JES), and transient pressure test article (TPTA). These short-burn duration tests simulated motor ignition transients and joint pressurization. Finally, flaws were tested in full-scale, full-duration static test motors, a qualification motor (QM-6), and a production verification motor (PVM-1). These tests are briefly described below.

*Seventy-Pound Charge (SPC) Motor*

Dozens of static tests were conducted using subscale motors in the SPC program.[8] The test article was designed to simulate the axial gas flow near the field joint in the SRM and to evaluate various field joint insulation configurations with and without O-ring and bondline defects. Multiple sets of the subscale hardware permitted an expedited program that provided the necessary test experience and design confidence to place flaws in full-scale hardware.

*Joint Environment Simulator (JES)*

The JES test article was formed from three full-diameter cylinders, each insulated and loaded with inert propellant (Fig. 11). Forward and aft domes formed the ends. A burning propellant cartridge in the upper section and burning propellant slabs bonded around the joints simulated the pressure transient during the SRM ignition, deflecting the case and grain. The test article provided an upper test joint designated as A, and a lower test joint designated as B. Because of the short-duration burn time and inert propellant, the test articles were refurbished rapidly and reused.[9–11]

*Transient Pressure Test Article (TPTA)*

The TPTA test hardware was similar to JES, except a fourth inert loaded cylinder was added (Fig. 12). In addition to the motor pressurization transients simulated in JES, attach strut flight loads caused by the external tank were applied to TPTA. Test joint designations were identical to the JES.[12–15]

*Qualification Motor (QM-6)*

QM-6 was a full-scale, full-duration RSRM static test motor.[16] The center field joint contained the only intentional flaw, a wave defect carved out of the clevis insulation.

**Table 2 Type 2 defects to the primary O-ring seal**

| | Defect configuration circumference × width, in. | | Thermal results: Erosion of primary O-ring seal,[c] in. | | Thermal results: Metal damage[d] | |
|---|---|---|---|---|---|---|
| Test article | J-joint defect | CF O-ring | Predicted | Measured | Predicted | Measured |
| JES-3B (joint B) | Channel: 0.5 × 0.1 | 1.0 × 0.08 | None | None | None | None |
| JES-3C (joint B) | Channel: 0.5 × 0.1 | 1.0 × 0.1 | None | None | None | None |
| TPTA-1.2 (joint A) | Channel: 0.5 × 0.1 | 1.0 × 0.1 | None | None | None | None |
| TPTA-1.2 (joint B) | Channel: 0.5 × 0.1 | 1.0 × 0.1 | None | None | None | None |
| TPTA-2.1 (joint A) | Channel: 0.5 × 0.1 | 1.0 × 0.1 | None | None | None | None |
| TPTA-1.3[a] (joint A) | Channel: 0.5 × 0.1 | 1.0 × 0.1 | None | None | —— | None |
| TPTA-1.3[b] (joint B) | Channel: 0.5 × 0.1 | 1.0 × 0.1 | None | 0.003 | —— | None |
| PVM-1 (aft joint) | Channel: 0.5 × 0.1 | 1.0 × 0.1 | None | None | None | None |

[a]0.005–0.010-in. interference gap for full circumference. [b]0.005–0.010-in. interference gap for 2-in. circumference, 0.005-in. wire across primary O-ring seal, 2-in. gap in $V_2$ filler; all flaws are in-line. [c]Diametrical erosion. [d]Steel temperature greater than 1000°F.

**Table 3 Type 3 defects to the primary O-ring seal**

| | Defect configuration circumference × width, in. | | Thermal results: Erosion of primary O-ring seal,[a] in. | | Thermal results: Metal damage[b] | |
|---|---|---|---|---|---|---|
| Test article | J-joint defect | CF and primary O-ring | Predicted | Measured | Predicted | Measured |
| TPTA-2.2 (joint A) | Channel: 0.5 × 0.1 | 1.0 × 0.1 | None | None | None | None |
| TPTA-2.2 (joint B) | Channel: 0.5 × 0.1 | 1.0 × 0.1 | None | None | None | None |

[a]Diametrical erosion. [b]Steel temperature greater than 1000°F.

*Production Verification Motor (PVM-1)*

PVM-1 was a full-scale, full-duration RSRM static test motor.[17] The aft joint had a channel defect in the mating insulation bondline and a flaw in the CF O-ring. The center field joint had a channel defect in the mating insulation surface bondline.

*Test Results*

Wave defects, bondline channel defects, O-ring reduction defects, and interference gaps were tested in three types of tests. Type 1 had channel and wave bondline flaws. Type 2 included bondline channels and CF O-ring reduction defects, assuring pressure to the primary O-ring seal. In two tests, interference gaps were included. Type 3 added flaws to the primary O-ring seal assuring pressure to the secondary O-ring seal.

**Flaw Test Results**

*Type 1—J-Joint Bondline Defects*

Pressure-assuring flaws, 0.050 × 0.125 in., were tested in JES-3B and PVM-1 (Table 1) . Both tests resulted in erosion of the CF O-ring. The CF O-rings maintained a seal and the steel case was not damaged. The analytical predictions from ORING2[4] were within 10% of the test results. SINDA analyses which predicted no metal damage, were also varied by the testing. Metal damage was assumed to occur when the temperature of the steel case components exceeded 1000°F, the temperature at which steel strength begins to deteriorate.

Wave defects were tested in JES-3A and QM-6. The wave defect in joint B of FED-3A sealed. A similar wave defect in QM-6 did not seal, but the CF O-ring was not heat affected. The tests demonstrated that wave defects will not always seal during motor pressurization, but that the overall joint design is tolerant of these defects.

*Type 2—Pressure Assured to Primary O-ring*

Eight test cases where pressure assuring flaws directed chamber gases to the primary O-ring cavity are summarized in Table 2. Seven of the tests with in-line defects in the joint bondline and CF O-ring, including the full-scale, full-duration PVM-1 static test motor, resulted in no primary O-ring heat effects. Even though the pressurization of the $V_2$ volume (Fig. 4) increased thermal effects, no metal damage resulted.

Minor primary O-ring heat effect in the TPTA-1.3 joint B was caused by three compounded defects: a bondline channel, a CF O-ring reduction, and an interference gap between the inner clevis leg and the CF. The gap was 0.005–1.010 in. high by 2 in. wide and in-line with a $V_2$ filler gap, and the CF O-ring and insulation bondline defects. The primary O-ring sealed even though a 0.005-in. wire stretched across the seal surface. The minor primary O-ring damage (0.003-in. erosion) supports the analytical findings that a large interference gap with a narrow width in a full-scale full-duration motor would result in hot gases in the $V_2$ volume and primary O-ring erosion. No primary O-ring erosion was predicted for the TPTA test because the analysis was conducted without the $V_2$ filler gap. In the test, the $V_2$ filler gap helped channel the hot gas to the primary O-ring. There was no damage to the metal components of the joint because of the shortburn duration of the TPTA test.

The defects in joint A of TPTA-1.3 were similar to those of joint B, except that the interference gap extended for the full circumference of the joint. As predicted, pressure at ignition

closed the gap, spreading the gas jet, thus preventing any primary O-ring erosion.

*Type 3—Pressure Assured to Secondary O-ring*

The two test joints in TPTA-2.2, with pressure-assuring flaws to the secondary O-ring seal, resulted in no heat effect on the primary or secondary O-ring seals (Table 3). Much of the heat dissipation occurred as the gases spread through the metal-to-metal interference fit. ORING2 and SINDA predictions, which indicated that no primary or secondary O-ring seal damage and no metal damage would occur, were verified with the tests.

## Conclusions

The RSRM field joint was extensively analyzed and tested to ensure its survivability. All results show that the joint will perform as designed. The metal case, and the primary and secondary O-ring seals, will remain at ambient temperature during motor operation, assuring the sealing integrity of the joint.

Tests and analyses have also been completed with postulated flaws in the design. The ensuing results verified that the joint would perform satisfactorily even with the presence of these selected flaws.

The RSRM field joint is now considered the most reliable in the solid rocket motor industry. Launches to date, incorporating the RSRM redesigned field joint, confirm the reliability.

## References

[1]Perry, M., and Passman, J., "RSRM Internal Insulation Design Rationale Definition," TWR-16742, Rev. A, Morton Thiokol, Space Operations, Brigham City, UT, Aug. 1988.

[2]Hicken, S., and Passman J., "RSRM Internal Insulation Design Summary," TWR-18133, Rev. A, Morton Thiokol, Space Operations, Brigham City, UT, Sept. 1988.

[3]Passman, J., "RSRM Internal Insulation Development and Qualification Report," TWR-17247, Rev. B, Morton Thiokol, Space Operations, Brigham City, UT, Sept. 1988.

[4]Maw, J. F., "Case Field Joint Redesign Flow/Thermal Analysis," Morton Thiokol, Inc., Brigham City, UT, TWR-17015 Rev. B, Aug. 1988.

[5]Boraas, S., "Thermal Effects of Noninterference Fit in the RSRM Case Field Joint," TWR-17910, Morton Thiokol, Space Operations, Brigham City, UT, Jan. 1988.

[6]Gruet, L., and O'Malley, M., "Floe/Thermal Analysis For PV-1 Test Motor," TWR-18264, Morton Thiokol, Space Operations, Brigham City, UT, July 1988.

[7]Gruet, L., "Comparison of Triangular and Rectangular Shaped Interference Gaps at the RSRM Field Joints," Morton Thiokol, Brigham City, UT, Memo L213-FY89-MO58, Oct. 1988.

[8]O'Malley, M., "Predicting RSRM Joint Volume Pressurization, Temperature Transients, and Ablation," *Journal of Spacecraft and Rockets,* Vol. 26, No. 6, Nov.-Dec. 1989, pp. 465-473.

[9]Knab, D., and Brinkerhoff, J., "Seventy-Pound Charge (SPC) Subscale Test Final Report," TWR-16845, Morton Thiokol, Space Operations, Brigham City, UT, Oct. 1988.

[10]Rubello, C., "Joint Environment Simulator 3A (JES-3A) Final Report," TWR-16501, Morton Thiokol, Space Operations, Brigham City, UT, Jan. 1987.

[11]Rubello, C., "Joint Environment Simulator 3B (JES-3B) Final Test Report," TWR-16534, Morton Thiokol, Space Operations, Brigham City, UT, Jan. 1988.

[12]Rubello, C., "Joint Environment Simulator 3C (JES-3C) Final Test Report," TWR-18000, Morton Thiokol, Space Operations, Brigham City, UT, Sept. 1988.

[13]Rubello, C., "Transient Pressure Test Article 1.2 (TPTA-1.2) Final Test Report," TWR-18075, Morton Thiokol, Space Operations, Brigham City, UT, April 1988.

[14]Rubello, C., "Transient Pressure Test Article 1.3 (TPTA-1.3) Final Test Report," TWR-18624, Morton Thiokol, Space Operations, Brigham City, UT, Oct. 1988.

[15]Rubello, C., "Transient Pressure Test Article 2.1 (TPTA-2.1) Final Test Report," TWR-17562, Morton Thiokol, Space Operations, Brigham City, UT, May 1988.

[16]Rubello, C., "Transient Pressure Test Article 2.2 (TPTA-2.2) Final Test Report," TWR-18428, Morton Thiokol, Space Operations, Brigham City, UT, July 1988.

[17]Magnum, K., "Space Shuttle Qualification Motor No. 6 (QM-6)," TWR-17372, Morton Thiokol, Space Operations, Brigham City, UT, June 1988.

[18]Garecht, D., "Space Shuttle Production Verification Motor 1 (PV-1) Final Test Report," TWR-17592, Morton Thiokol, Space Operations, Brigham City, UT, Oct. 1988.